VIP Gold Catalysis

DOI: 10.1002/ange.201107391

Imaging Isolated Gold Atom Catalytic Sites in Zeolite NaY**

*Jing Lu, Ceren Aydin, Nigel D. Browning, and Bruce C. Gates**

Gold, the most stable metallic element, attracted wide attention as a catalyst only after the discovery that gold nanoclusters on oxide supports are highly active and selective for reactions including numerous oxidation,[1–8] hydrogenation,[9–11] hydroamination,[12,13] ring expansion,[14,15] and coupling[16,17] reactions. The catalytic properties of supported gold strongly depend on the gold–support interactions and the size of the active species, which must be small—typically clusters with diameters of the order of 1 nm.[18–20] Frequent discoveries of new gold-catalyzed reactions are leading the science; understanding has been slow to emerge.[21] Major challenges are to identify the catalytically active species and to characterize gold–support interactions.

Recent advances in aberration-corrected scanning transmission electron microscopy (STEM) of supported metal complexes and clusters,[22–26] including gold,[27–29] have allowed imaging with atomic resolution. The images provide direct local information about the catalytic species that was not attainable with spectroscopic and traditional microscopic techniques. For example, Herzing et al.[27] inferred from catalyst performance data and aberration-corrected STEM images that the activity for CO oxidation of gold supported on FeO_x is associated with bilayer gold clusters comprising less than 10 atoms, which were found to be much more active than the numerous other gold species in the samples, including some with structures only slightly different from those inferred to be the most active.

Such nanoclusters are not the only active supported gold catalysts—and not the simplest—even isolated mononuclear cationic gold complexes on supports have been inferred to be active for CO oxidation,[30] and, similarly, numerous cationic gold complexes in solution are catalytically active.[31,32] Isolated cationic gold species on supports have limited stability and are challenging to characterize,[33,34] but their structural simplicity (in contrast to the complexity of almost all supported gold catalysts,[27,35–37] exemplified by the images of Herzing et al.[27]) commends them to investigations by STEM. Such investigations can be facilitated by the use of porous supports with highly uniform structures, such as crystalline aluminosilicates (zeolites).[38] Zeolites offer surface sites with uniformities that are unattainable on high-area oxide surfaces, which are inherently heterogeneous.[39]

We now report how aberration-corrected STEM can be used to characterize atomically dispersed gold in a zeolite—notwithstanding the relative instability of both the gold species and the zeolite itself under the influence of the electron beam.[28,40,41] We show that site-isolated mononuclear gold complexes are catalytic sites for CO oxidation.

A fruitful approach to the synthesis of highly dispersed, uniform gold species on surfaces involves the reactive precursor $Au(CH_3)_2(acac)$ (acac is acetylacetonate), which interacts strongly with oxides and zeolites.[42,43] In contrast, traditional syntheses with gold salts generally lead to nonuniform gold particles with diameters exceeding a few nanometers.[44,45] When the supports are zeolites, these gold particles generally form on the external crystallite surfaces, because they are too large to fit in the pores.[44]

Adsorption of $Au(CH_3)_2(acac)$ on zeolite NaY was inferred to lead to mononuclear gold complexes within the intracrystalline cages,[46] but the only evidence is spectroscopic (infrared, IR, and extended X-ray absorption fine structure, EXAFS), and in the absence of images we cannot rule out the presence of a minority of gold species, such as clusters—and such species could be catalytically active.[27]

Recently, Ortalan et al.[47] showed that STEM can be used to determine the locations of iridium atoms and nanoclusters within the pores of a faujasite zeolite (ultrastable HY, USY). However, Ortalan's technique was limited by the low-dose imaging conditions, chosen because of the susceptibility of the zeolite to beam damage in the microscope. Ortalan's images, characterized by low signal-to-noise ratios, required extensive image processing and simulations. Consequently, most of his conclusions were drawn on the basis of simulated images, which can be affected by artifacts introduced during the processing and simulations.[48]

Here we show how STEM images obtained under high-dose conditions identify and determine the locations of isolated gold complexes in zeolite NaY and demonstrate that they are catalytically active sites for CO oxidation. The sample was prepared from $Au(CH_3)_2(acac)$[46] and the zeolite NaY (Si/Al ratio = 2.5, atomic), with the gold loading being 1 wt%. This zeolite is less stable than the aforementioned USY zeolite (Si/Al ratio = 30, atomic)[49,50] and therefore more difficult to image. However, it offers the benefit of a much higher degree of crystallinity and uniformity than the USY zeolite[51,52] and hence more readily identifiable surface sites for the gold.

[*] J. Lu,[+] C. Aydin,[+] Prof. N. D. Browning,[$] Prof. B. C. Gates
Department of Chemical Engineering and Materials Science
University of California
One Shields Avenue, Davis, CA 95616 (USA)
E-mail: bcgates@ucdavis.edu
Homepage: http://www.chms.ucdavis.edu/research/web/catalysis

[$] Current address:
Fundamental and Computational Sciences Division
Pacific Northwest National Laboratory
902 Battelle Boulevard, Richland, WA 99352 (USA)

[+] These authors contributed equally to this work.

[**] This work was supported by the Department of Energy (DOE) Basic Energy Science, grant number DE-FG02-04ER15513 (J.L.), and grant number DE-FG02-03ER46057 (C.A.), and the University of California Lab Fee Program.

Supporting information for this article is available on the WWW under http://dx.doi.org/10.1002/anie.201107391.

Images were obtained with a JEOL JEM-2100F electron microscope operated at 200 kV (imaging dose around $10^5\ e^-\ Å^{-2}$). The high-resolution images, recorded within seconds, before the onset of sample damage by the electron beam, and with high signal-to-noise ratios, do not share the limitations of Ortalan's low-dose images.[47] They provide direct structural characterizations of the gold–support interface and demonstrate the crystallographic locations of the gold atoms in the zeolite.

Figures 1 and 2 are STEM images, acquired in the high-angle annular dark-field (HAADF) detection mode, of the catalyst before and after use for CO oxidation in a once-through flow reactor. In this imaging mode, the intensity of the dominant scattering mechanism that gives rise to the contrast is proportional to the square of the atomic number (Z^2) of the element.[53] Thus, single gold atoms ($Z=79$) appear as bright centers (e.g., Figure 2, in the dashed rectangles) in the zeolite framework consisting of light atoms: Si ($Z=14$), Al ($Z=13$), Na ($Z=11$), and O ($Z=8$). The images shown in Figures 1 A, B and 2 and their fast Fourier transforms (FFTs) match the simulated framework and diffraction pattern characterizing the [100], [111], and [110] orientations of the zeolite, respectively, indicating that the crystallites were imaged undamaged in these orientations.

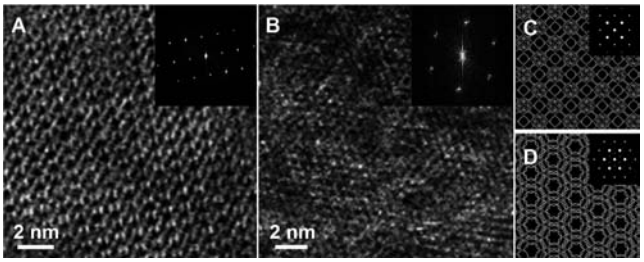

Figure 1. A and B) Aberration-corrected HAADF-STEM images of the sample prepared by adsorption of $Au(CH_3)_2(acac)$ in zeolite NaY in the [100] (A) and [111] (B) projections. C and D) Simulated frameworks and theoretical diffraction patterns of zeolite Y in the [100] (C) and [111] (D) projections.

The interpretation of the images is much easier for the [110] projection than for the [100] and [111] projections, because in the [110] projection there is minimal framework overlap, with the images providing a direct view to the insides of supercages through 12-ring apertures (channel openings). Arrays of cavities with hexagonal arrangements are highlighted with white circles in Figure 2 A and B, matching precisely the simulated zeolite Y framework lattice in the [110] projection (Figure 2 E). The orientation of the lattice in each image is parallel to the patterns in the corresponding FFTs (compare the white circles in Figure 2 A and B with the white dots in Figure 2 C and D).

The images in Figures 1 and 2 show that the gold atoms are atomically dispersed, with no evidence of gold clusters. Images recorded at lower magnifications (Figure S2 in the Supporting Information) further confirm the absence of clusters. These observations are consistent with EXAFS data[46,54] characterized by a lack of discernable Au–Au contributions. We infer that the atomic dispersion of the gold is stabilized by the site isolation of the atoms in the zeolite—the images indicate that only less than 5% of the zeolite cages contained more than one gold atom.

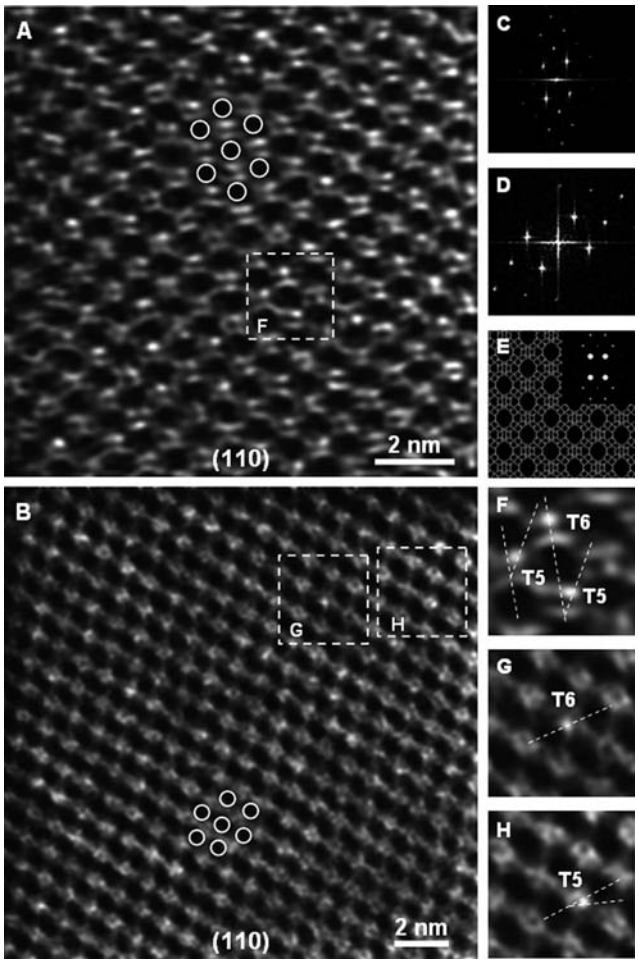

Figure 2. Aberration-corrected HAADF-STEM images of the sample prepared by adsorption of $Au(CH_3)_2(acac)$ in zeolite NaY. A) Initially prepared sample. B) Sample after treatment in flowing $CO+O_2$ (during CO oxidation catalysis) for 30 min. C) FFT of the experimental image shown in (A). D) FFT of the experimental image shown in (B). E) Simulated framework and theoretical diffraction pattern of zeolite Y in the [110] projection. F–H) Zoomed-in views of the regions shown in rectangles in (A) and (B).

The images of Figure 2 identify two distinct bonding sites for gold complexes, namely T5 and T6 sites (Figure 3 illustrates what is meant by the designations of these sites). Bonding of metal atoms at T5 and T6 sites was predicted by calculations at the level of density functional theory (DFT).[53] When viewed from the [110] projection of the zeolite crystal, the sites aligned along the central axis of the cavities of the zeolite lattice are T6 sites, and those aligned in the diagonal direction with respect to the central axis are T5 sites (Figure 2 F–H).

Figure 2 A and B, respectively, show the initially prepared catalyst and the catalyst after treatment in flowing $CO+O_2$ (during CO oxidation catalysis) at 298 K and 1 bar for 30 min in a once-through flow reactor ($P_{CO}=P_{O_2}=16$ mbar, bal-

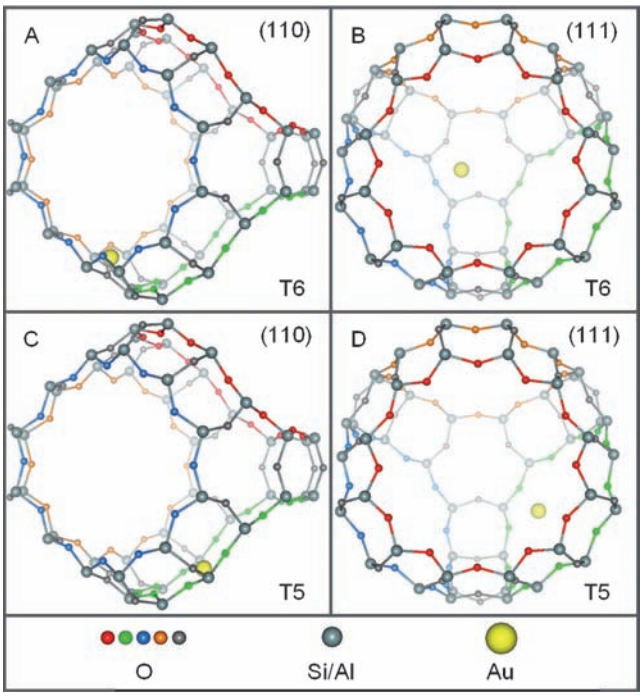

Figure 3. A and B) Perspective views of gold atoms at T6 positions in an isolated faujasite supercage, viewed from the [110] and [111] projections. C and D) Perspective views of gold atoms at T5 positions in an isolated supercage, viewed from the [110] and [111] projections.

anced with helium); the catalyst performance matched that reported by Fierro-Gonzalez et al.[46] Examination of all the gold atoms evident in the images (Figure 2 A and B) showed that approximately 34 % of the gold complexes in the initially prepared sample resided at T6 sites and that this value increased to 73 % after CO oxidation catalysis.

A more detailed understanding of these sites in the crystallographic structure of the zeolite is provided by Figure 3 A and C, which are perspective views of a supercage from the [110] projection—the same as that of the images in Figure 2. The gold atoms evident in Figure 2 A and C represent those in T5 and T6 sites, as shown in the images exemplified by Figure 2 F. To illustrate the three-dimensional structure of the faujasite supercage, the oxygen atoms of the four 12-membered ring apertures are highlighted in color. The same two supercages in Figure 3 A and C are rotated to the [111] orientation in Figure 3 B and D, where the internal space of the supercages can be seen directly through the apertures normal to the direction of view (highlighted in red). As shown in Figure 3 A and C, the overlap of apertures highlighted in blue and orange creates the appearance of a cavity in the experimental image (see Figure S1 in the Supporting Information for a model with more than one supercage unit). The [110] projection view (Figure 3 A) shows a gold atom at a T6 site located in the space inside the supercage and between the bottom part of the blue and orange apertures. The view from the [111] projection (Figure 3 B) shows that the T6 site is atop the six-membered ring created between blue, orange, and green apertures. On the other hand, views from both the [110] and [111] projections (Figure 3 C and D) show that the gold atoms in the T5 sites are approximately in the same plane as the aperture highlighted in green. On the basis of this analysis, we conclude that the gold atoms appearing at T6 and T5 positions are inside the supercages, and those at T5 positions are closer to the channel openings connecting adjacent supercages.

Time-resolved EXAFS and IR spectra characterizing the catalyst in the working state indicated that the precursor $Au(CH_3)_2(acac)$ was initially physisorbed at the aluminum sites of the zeolite surface (Figure 4 A),[46,54] likely interacting

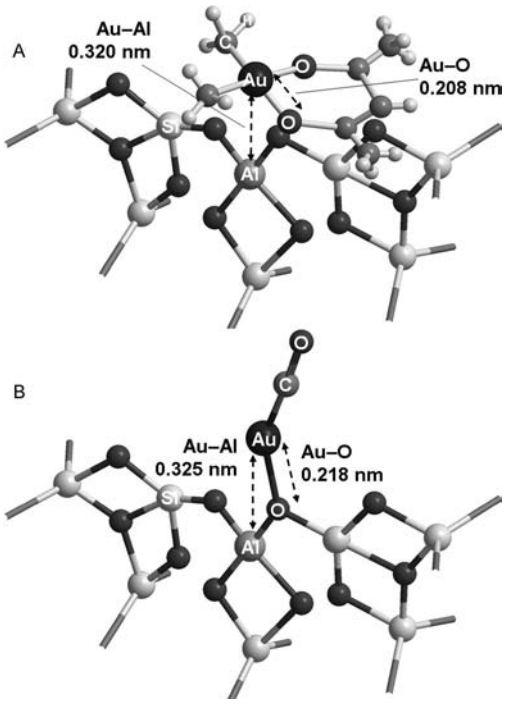

Figure 4. Structural models of physisorbed $Au(CH_3)_2(acac)$ on the zeolite surface (A) and Au(CO) complex bonded to the zeolite framework (B). The structures were inferred from the STEM images and EXAFS and IR data.

with the surface by hydrogen bonding.[56] Upon contact with CO and O_2, the acac ligands were rapidly detached from the gold, leading to the formation of chemisorbed gold complexes, each bonded to approximately one zeolite oxygen atom (Figure 4 B).[56]

The transformation of the gold complexes from physisorbed $Au(CH_3)_2(acac)$ into chemisorbed species in the presence of $CO + O_2$ was accompanied by the replacement of the CH_3 ligands by CO, as shown by the replacement of the $Au–C_{methyl}$ and $Au–O_{acac}$ contributions by $Au–C_{carbonyl}$ and $Au–O_{carbonyl}$ contributions in the EXAFS spectrum and by the appearance of a 2169 cm^{-1} band in the IR spectrum (which is assigned to CO bonded to gold). These changes correspond to changes in the gold from approximately Au^{III} to Au^{I}, as indicated by an increase of the white line intensity in the X-ray absorption near edge spectra (XANES).[46,54,57] Consistent with these inferences, the appearance of an $Au–O_{zeolite}$ contribution was indicated by the EXAFS data, indicating the formation of gold–support bonds.[46,54]

These results, together with the STEM observation that the site-isolation of the gold complexes was retained after CO oxidation catalysis, support the inference that the gold species were stabilized by their confinement in the zeolite channels.

The rate of the catalytic CO oxidation reaction characterizing the zeolite containing Au^{III} was reported[46] to be $(2.6 \pm 0.3) \times 10^{-2}$ mol of CO_2 (mol of $Au \times s)^{-1}$. After approximately 15 min of operation in the flow reactor, the reaction rate had decreased to $(2.9 \pm 0.2) \times 10^{-3}$ mol of CO_2 (mol of $Au \times s)^{-1}$ as gold species were transformed from Au^{III} to Au^{I}.[46] Thus, these results show a significant change in the catalytic activity attributed to changes in the oxidation state of the gold,[46,57] but it had heretofore been unclear whether formation of gold clusters from a small fraction of the gold atoms had occurred. Our data show that the mononuclearity of the gold species was retained after catalysis, and the STEM observations show that the change in the gold oxidation state was associated with the movement of some of the gold complexes from T5 to T6 sites and a change in the gold–support interface. This inference is consistent with the reported[46,54] EXAFS and IR spectra. These data, combined with the lack of STEM evidence of gold clusters weigh strongly against the possibility that gold clusters were responsible for the catalytic activity.[27]

In summary, the results show that the use of a crystalline zeolite support and a reactive organogold precursor leads to an atomically dispersed gold catalyst with a high degree of uniformity that can be characterized precisely with atomic-resolution STEM complemented by spectroscopy. Our STEM images, combined with reported spectra, identify the catalytic sites as site-isolated gold complexes and indicate that the observed change in activity during operation of the catalyst is associated with a change in the gold–support interface. Thus, aberration-corrected STEM can be used to probe the metal–support interface in the most highly dispersed supported metal catalysts, even when they consist of beam-sensitive materials. We anticipate rapid advances in the atomic-scale understanding of supported catalysts incorporating heavy-metal-atom complexes and small metal clusters.

Experimental Section

The samples were prepared and handled with standard Schlenk line, glovebox, and glovebag techniques with exclusion of moisture and air. The zeolite NaY (Zeolyst International, CBV100) powder (Si/Al: 2.5) was calcined in flowing O_2 (Airgas, 99.2%) at 573 K for 4 h followed by evacuation for 16 h at 573 K. It was isolated and stored in a glovebox (MBraun) filled with ultrahigh-purity argon (Praxair, Grade 5.0). Prior to synthesis of the catalyst precursor $Au(CH_3)_2$-(acac), *n*-pentane solvent (Fisher Scientific, HPLC grade) was dried and purified in chromatographic columns containing activated Al_2O_3 and activated Al_2O_3-supported copper in a Grubbs apparatus (MBraun) and deoxygenated by sparging with argon (Airgas, UHP, Grade 5.0). To prepare the supported gold complex, $Au(CH_3)_2$(acac) (Strem, 98%) mixed with the calcined zeolite in a Schlenk flask was slurried in dried *n*-pentane at 298 K for one day. The solvent was then removed by evacuation for one day. The resultant powder, containing 1 wt% Au, was stored in a glovebox.

Catalytic CO oxidation experiments were performed with a once-through flow reactor with an online gas chromatograph (Hewlett–Packard, HP-589 Series II) under the conditions reported.[46]

In the STEM experiments, to minimize the exposure to air and moisture, powder samples were loaded onto a lacey carbon, 300-mesh copper grid (Ted-Pella) in the glovebox. The grid in the glovebox was packed in an Eppendorf tube and sealed with Parafilm. Each Eppendorf tube was placed in a Swagelok stainless-steel tube sealed with O-rings for transfer to the microscope. There, an argon-filled glovebag (Glas-Col) was purged five times with ultrahigh purity argon, and the TEM grid was loaded onto the TEM holder in the glovebag under a blanket of flowing argon. As argon flowed over the TEM holder, it was transferred from the glovebag to the microscope with an air exposure of at most 4 s.

Images were obtained with a JEOL JEM-2100F electron microscope equipped with an FEG, operated at 200 kV, with a CEOS hexapole probe (STEM) aberration corrector. The images were captured by a HAADF detector with a collection semi-angle of 75–200 mrad and a probe convergence semi-angle of 17.1 mrad. The imaging dose was approximately 10^5 $e^- Å^{-2}$. Prior to imaging of the samples, the aberration corrector was aligned with a Pt/Ir on holey carbon standard sample (SPI supplies) until atomic resolution of the metals was achieved (Figure S3 in the Supporting Information) and the lattice spacings of the metals were confirmed. Images were obtained in < 5 s including instrument optimization prior to image acquisition, before the occurrence of electron beam damage of the zeolite framework and gold atoms. Figure S4 in the Supporting Information shows an image of the same area shown in Figure 2 A, obtained after 20 s of beam exposure, indicating that the zeolite framework had been substantially destroyed by the electron beam.

Received: October 20, 2011
Published online: March 12, 2012

Keywords: electron microscopy · gold · interfaces · zeolites

[1] M. Haruta, N. Yamada, T. Kobayashi, S. Iijima, *J. Catal.* **1989**, *115*, 301 – 309.
[2] M. Haruta, S. Tsubota, T. Kobayashi, H. Kageyama, M. J. Genet, B. Delmon, *J. Catal.* **1993**, *144*, 175 – 192.
[3] M. Haruta, *Nature* **2005**, *437*, 1098 – 1099.
[4] P. Ionita, B. C. Gilbert, V. Chechik, *Angew. Chem.* **2005**, *117*, 3786 – 3788; *Angew. Chem. Int. Ed.* **2005**, *44*, 3720 – 3722.
[5] L. Prati, M. Rossi, *Catal. Today* **1997**, *110*, 509 – 516.
[6] S. Carrettin, P. McMorn, P. Johnston, K. Griffin, G. J. Hutchings, *Chem. Commun.* **2002**, 696 – 697.
[7] S. Carrettin, P. McMorn, P. Johnston, K. Griffin, C. J. Kiely, G. A. Attard, G. J. Hutchings, *Top. Catal.* **2004**, *27*, 131 – 136.
[8] M. Comotti, C. Della Pina, R. Matarrese, M. Rossi, *Angew. Chem.* **2004**, *116*, 5936 – 5939; *Angew. Chem. Int. Ed.* **2004**, *43*, 5812 – 5815.
[9] A. Corma, C. Gonzalez-Arellano, M. Iglesias, F. Sanchez, *Appl. Catal. A* **2009**, *356*, 99 – 102.
[10] J. E. Bailie, G. J. Hutchings, *Chem. Commun.* **1999**, 2151 – 2152.
[11] A. Corma, P. Serna, *Science* **2006**, *313*, 332 – 334.
[12] N. Nishina, Y. Yamamoto, *Angew. Chem.* **2006**, *118*, 3392 – 3395; *Angew. Chem. Int. Ed.* **2006**, *45*, 3314 – 3317.
[13] A. Corma, P. Concepción, I. Domínguez, V. Fornés, M. J. Sabater, *J. Catal.* **2007**, *251*, 39 – 47.
[14] A. Stephen, K. Hashmi, T. M. Frost, J. W. Bats, *J. Am. Chem. Soc.* **2000**, *122*, 11553 – 11554.
[15] S. Carrettin, M. C. Blanco, A. Corma, A. S. K. Hashmi, *Adv. Synth. Catal.* **2006**, *348*, 1283 – 1288.
[16] C. González-Arellano, A. Corma, M. Iglesias, F. Sanchez, *J. Catal.* **2006**, *238*, 497 – 501.
[17] C. González-Arellano, A. Abad, A. Corma, H. Garcia, M. Iglesias, F. Sanchez, *Angew. Chem.* **2007**, *119*, 1558 – 1560; *Angew. Chem. Int. Ed.* **2007**, *46*, 1536 – 1538.
[18] M. Haruta, *Catal. Today* **1997**, *36*, 153 – 166.

[19] A. Abad, A. Corma, H. Garcia, *Chem. Eur. J.* **2008**, *14*, 212 – 222.
[20] M. Boronat, A. Corma, *Dalton Trans.* **2010**, *39*, 8538 – 8546.
[21] A. S. K. Hashmi, G. J. Hutchings, *Angew. Chem.* **2006**, *118*, 8064 – 8105; *Angew. Chem. Int. Ed.* **2006**, *45*, 7896 – 7936.
[22] A. Uzun, V. Ortalan, N. D. Browning, B. C. Gates, *Chem. Commun.* **2009**, 4657 – 4659.
[23] A. Kulkarni, M. Chi, V. Ortalan, N. D. Browning, B. C. Gates, *Angew. Chem.* **2010**, *122*, 10287 – 10290; *Angew. Chem. Int. Ed.* **2010**, *49*, 10089 – 10092.
[24] V. Ortalan, A. Uzun, B. C. Gates, N. D. Browning, *Nat. Nanotechnol.* **2010**, *5*, 843 – 847.
[25] F. L. Deepak, R. Esparza, B. Borges, X. Lopez-Lozano, M. Jose-Yacaman, *ACS Catal.* **2011**, *1*, 537 – 543.
[26] L. P. Hansen, Q. M. Ramasse, C. Kisielowski, M. Brorson, E. Johnson, H. Topsøe, S. Helveg, *Angew. Chem.* **2011**, *123*, 10335 – 10338; *Angew. Chem. Int. Ed.* **2011**, *50*, 10153 – 10156.
[27] A. A. Herzing, C. J. Kiely, A. F. Carley, P. Landon, P. G. J. Hutchings, *Science* **2008**, *321*, 1331 – 1335.
[28] A. Uzun, V. Ortalan, Y. Hao, N. D. Browning, B. C. Gates, *J. Phys. Chem. C* **2009**, *113*, 16847 – 16849.
[29] J. Sá, A. Goguet, S. F. R. Taylor, R. Tiruvalam, C. J. Kiely, M. Nachtegaal, G. J. Hutchings, C. Hardacre, *Angew. Chem.* **2011**, *123*, 9074 – 9078; *Angew. Chem. Int. Ed.* **2011**, *50*, 8912 – 8916.
[30] J. Guzman, B. C. Gates, *J. Am. Chem. Soc.* **2004**, *126*, 2672 – 2673.
[31] D. J. Gorin, F. D. Toste, *Nature* **2007**, *446*, 395 – 403.
[32] A. S. K. Hashmi, *Gold Bull.* **2003**, *36*, 3 – 9.
[33] G. C. Bond, C. Louis, D. T. Thompson, *Catalysis by Gold*, Imperial College Press, London, **2007**.
[34] A. Corma, H. Garcia, *Chem. Soc. Rev.* **2008**, *37*, 2096 – 2126.
[35] A. Tompos, J. L. Margitfalvi, E. G. Szabó, Z. Pa'szti, I. Sajó, G. J. Radnóczi, *J. Catal.* **2009**, *266*, 207 – 217.
[36] S. N. Rashkeew, A. R. Lupini, S. H. Overbury, S. Pennycook, S. T. Pantelides, *Phys. Rev. B* **2007**, *76*, 035438-1 – 035438-8.
[37] J. E. Bailie, G. J. Hutchings, *Catal. Commun.* **2001**, *2*, 291 – 294.
[38] M. E. Davis, *Nature* **2002**, *417*, 813 – 821.
[39] J. O. Ehresmann, P. W. Kletnieks, A. Liang, V. A. Bhirud, O. P. Bagatchenko, E. J. Lee, M. Klaric, B. C. Gates, J. F. Haw, *Angew. Chem.* **2006**, *118*, 588 – 590; *Angew. Chem. Int. Ed.* **2006**, *45*, 574 – 576.
[40] L. A. Bursill, J. M. Thomas, K. J. Rao, *Nature* **1981**, *289*, 157 – 158.
[41] E. H. Hirsch, *Nature* **1981**, *293*, 759.
[42] M. Baltes, O. Collart, P. Van Der Voort, E. F. Vansant, *Langmuir* **1999**, *15*, 5841 – 5845.
[43] P. Van Der Voort, M. B. Mitchell, E. F. Vansant, M. G. White, *Interface Sci.* **1997**, *5*, 169 – 197.
[44] J.-N. Lin, J.-H. Chen, C.-Y. Hsiao, Y.-M. Kang, B.-Z. Wan, *Appl. Catal. B* **2002**, *36*, 19 – 29.
[45] G. Li, J. Edwards, A. F. Carley, G. J. Hutchings, *Catal. Commun.* **2007**, *8*, 247 – 250.
[46] J. C. Fierro-Gonzalez, B. C. Gates, *J. Phys. Chem. B* **2004**, *108*, 16999 – 17002.
[47] V. Ortalan, A. Uzun, B. C. Gates, N. D. Browning, *Nat. Nanotechnol.* **2010**, *5*, 506 – 510.
[48] J. P. Buban, Q. Ramasse, B. Gipson, N. D. Browning, H. Stahlberg, *J. Electron Microsc.* **2010**, *59*, 103 – 112.
[49] G. T. Kerr, *Adv. Chem. Ser.* **1973**, *121*, 219 – 229.
[50] H. Miessner, H. Kosslick, U. Lohse, B. Parlitz, V.-A. Tuan, *J. Phys. Chem.* **1993**, *97*, 9741 – 9748.
[51] A. H. Janssen, A. J. Koster, K. P. de Jong, *Angew. Chem.* **2001**, *113*, 1136 – 1138; *Angew. Chem. Int. Ed.* **2001**, *40*, 1102 – 1104.
[52] K. P. de Jong, J. Zečević, H. Friedrich, P. E. de Jongh, M. Bulut, S. van Donk, R. Kenmogne, A. Finiels, V. Hulea, F. Fajula, *Angew. Chem.* **2010**, *122*, 10272 – 10276; *Angew. Chem. Int. Ed.* **2010**, *49*, 10074 – 10078.
[53] S. J. Pennycook, D. E. Jesson, *Ultramicroscopy* **1991**, *37*, 14 – 38.
[54] J. C. Fierro-Gonzalez, B. C. Gates, *Langmuir* **2005**, *21*, 5693 – 5695.
[55] J. F. Goellner, B. C. Gates, G. N. Vayssilov, N. Rösch, *J. Am. Chem. Soc.* **2000**, *122*, 8056 – 8066.
[56] M. Hisamoto, R. C. Nelson, M.-Y. Lee, J. Eckert, S. L. Scott, *J. Phys. Chem. C* **2009**, *113*, 8794 – 8805.
[57] J. C. Fierro-Gonzalez, B. G. Anderson, K. Ramesh, C. P. Vinod, J. W. Niemantsverdriet, B. C. Gates, *Catal. Lett.* **2005**, *101*, 265 – 274.